Electronic and structural properties of oligophenylene ethynylenes on Au(111) surfaces

Ling Miao
Department of Chemical Engineering, Texas A&M University, College Station, Texas 77840

Jorge M. Seminario
Department of Chemical Engineering, Texas A&M University, College Station, Texas 77840 and Department of Electrical and Computer Engineering, A&M University, College Station, Texas 77840

(Received 16 February 2007; accepted 27 March 2007; published online 11 May 2007)

The interaction of oligophenylene ethynylene (OPE) on the (111) surface of a gold slab resembling a self-assembled monolayer (SAM) is investigated using *ab initio* density functional theory calculations. The authors performed a full optimization including all atoms in the OPE and in the slab to better understand OPE adsorption on the surface. It is found that OPE has two energetically favorable adsorption sites on the Au surface with relatively different molecular geometries: the nontop site adsorption greatly modifies the (111) surface structure; however, the extensive electron interactions enable a delocalized electron density distribution, implying an improved conductivity between OPE and Au, and the top site which is 0.9 eV higher in energy than the nontop and features weaker Au–S bonds. Interestingly the on top configuration shows a strong spin imbalance along the molecule and the nontop shows a small spin imbalance on the surface. This feature is of strong interest for the development of resonators for the detection of chemical and biological agents. They have also calculated the frequency spectrum of these SAMs, which yield deformations in the gold surface yielding peak frequency shifts specific to each absorption site. © *2007 American Institute of Physics*. [DOI: 10.1063/1.2734545]

I. INTRODUCTION

Recently, phenylene ethynylene based oligoderivatives have attracted considerable interest in both experimental and theoretical research owing to their potential applications in molecular electronic devices, such as electrical switching,[1] memory cells,[2,3] molecular wires,[4] and rectifiers.[5] These works showed that oligophenylene ethynylene (OPE) (Fig. 1) and derivatives can be used to tailor their current-voltage characteristics, because their electronic transport properties vary significantly based on the molecular configuration, moiety, neighbor environment, as well as on the contact structure.[6–18] Recent studies also provided insight into the coupling between charge carriers and vibrational motion of the molecule.[18–20] In addition to the applications in diverse electronic devices, OPEs have also been widely investigated as optical and optoelectronic devices thanks to their vibrational relaxation under molecular conformational changes.[21–24] The high-energy vibrational modes from the interphenyl ring stretching as well as the low-energy vibrational modes from torsional twisting are especially essential for the emission and absorption spectra of the molecule,[25] and significantly affect the photophysical characteristics.[26] Therefore, the investigation of molecular vibrations is also important to the understanding of various properties of OPE and critical to molecular device properties.

Experimentally, self-assembled monolayers (SAMs) of OPEs are usually assembled onto a lithographically fabricated bottom contact, typically an Au (111) surface, through organic thiols and then topped by Au or other metal contact using thermal evaporation.[1,27,28] Theoretically, due to the great interest in the electronic property changes with the morphology of the OPE and the functional groups, computational analyses have been performed to the OPE or similar systems regarding their structure and conductivity.[29–34] In these works, density functional theory (DFT) and Green's functions were applied to the study of electron transport through these π-conjugated molecules attached to Au atoms, whereby molecular frontier orbitals such as the highest occupied molecular orbital and lowest unoccupied molecular orbital and others in their neighborhood are used to predict the electrical characteristics of the molecules.

In this paper, we study the structural, electronic, and vibrational properties of OPE on the Au(111) surface using plane wave based DFT calculations. Theoretical studies of OPE systems were restricted to isolated molecules until a combined DFT-Green's function approach was used for a dinitro-OPE molecule.[35] Several other calculations followed, for instance.[34] Here, we consider an extended molecule-Au surface using periodic boundary conditions and a plane wave basis to understand the adsorption geometry of groups of OPE molecules as well as their electronic properties. We also investigate the influence of Au surface on the vibrational frequency of critical atoms along the molecular axis, such as C–C, C–H, and C–S bonds. Furthermore, we show that different adsorption sites have different effects on the surface vibrational frequency, which may be used as a method for the identification of the location of OPE molecules on the Au surface. Finally, we perform an analysis of spin polarization

 © 2007 American Institute of Physics

Downloaded 25 Sep 2007 to 165.91.226.76. Redistribution subject to AIP license or copyright, see http://jcp.aip.org/jcp/copyright.jsp

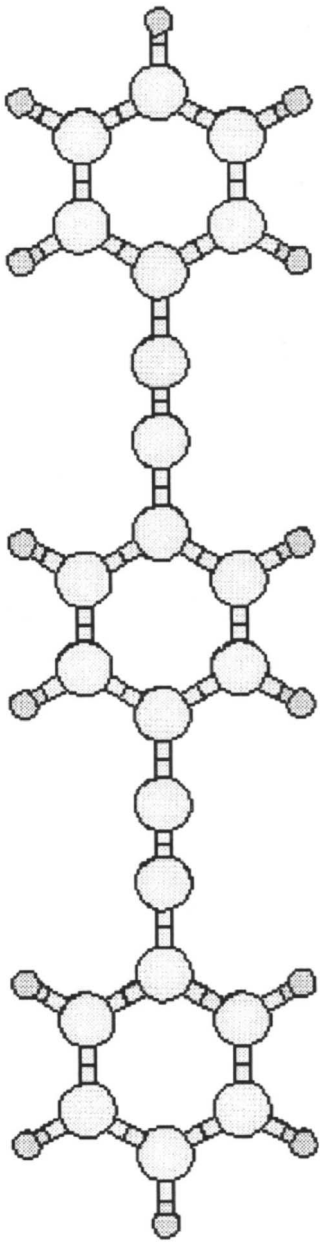

FIG. 1. Molecular structure of the oligophenylene ethynylene (OPE). Yellow and blue atoms represent carbon and hydrogen, respectively.

on the molecule and gold surfaces as this is an important feature for the development of magnetic sensors for chemical and biological agents.

II. METHODOLOGY

All calculations are performed using Vienna *ab initio* simulation package[36–39] (VASP) using density functional theory with the generalized gradient approximation (GGA) of Perdew and Wang[40] (PW91) and the projector augmented wave (PAW) potential.[41,42] Generally the PAW method is more accurate than the ultrasoft pseudopotential method because it reconstructs the exact valence wave function with all nodes in the core region. The plane wave basis set assumes a supercell geometry that is periodic in all three directions. Each OPE molecule and derivatives are considered to be isolated on an infinitely long Au wire, with a lateral separation of about 0.5 Å. The Brillouin zone of the supercell was sampled using the special Monkhorst-Pack[43] $7\times1\times1$ k points. A kinetic energy cutoff of 500 eV is used for the plane wave basis set. Structural configurations of all systems are optimized until residual forces are within 0.05 eV/Å.

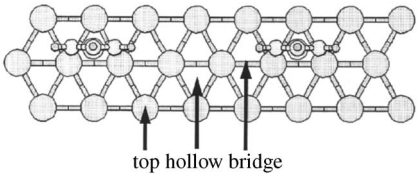

FIG. 2. Schematic drawing showing adsorption sites on the Au(111) surface. Two unit cells are shown.

III. RESULTS AND DISCUSSIONS

A. Geometries and energetics

The molecules are allowed to reach a stable conformation with the Au surface through organic thiols, which are known to chemisorb on gold as thiolates after the deprotonation of the S–H bonds. This has been widely used in forming self-assembled monolayers on gold surfaces.[44,45] Three adsorption sites, top, bridge, and hollow, are considered, where S atom is equally bonded to one, two, or three Au atoms, respectively, as shown in Fig. 2. The OPE is initially placed on each site before the geometry optimization. A conjugate-gradient algorithm is used to relax the nuclei into a local minimum configuration, followed by a single point energy calculation. By comparing the total energies at each adsorption site, the energetically favorable local minimum is obtained. From our calculations, we notice that the total energy of top site adsorption is ~0.9 eV higher than those of the

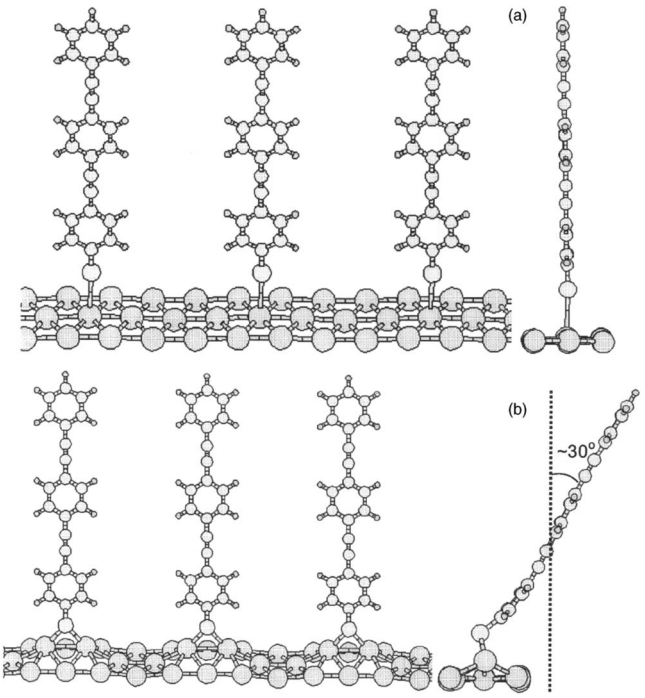

FIG. 3. Front view and side view of OPE thiolate adsorption on (a) top and (b) nontop sites of the Au(111) surface. Front views show three unit cells. OPE thiolate of nontop site yield an angle of ~30°.

Downloaded 25 Sep 2007 to 165.91.226.76. Redistribution subject to AIP license or copyright, see http://jcp.aip.org/jcp/copyright.jsp

TABLE I. Selected bond lengths and bond angle of the optimized OPE thiolate on Au(111) top and nontop sites. The nontop site is obtained from geometry optimizations starting with bridge and hollow sites; both optimizations yield very similar results.

	d_{Au-S} (Å)	d_{S-C} (Å)	θ_{Au-S-C} (deg)
Top	3.36	1.71	179.1
Nontop (bridge)	2.43	1.71	112.0
Nontop (hollow)	2.44	1.75	110.7

other two site adsorptions. OPE remains straight on the top site with a relatively larger distance to the Au surface, as shown in Fig. 3(a). The overall (111) surface structure remains except that the Au atoms below the S are slightly lifted up by about 0.2 Å from the surface plane. However, bridge and hollow site adsorptions have a much stronger effect on the morphology of the Au surface and the OPE molecule when compared to top site adsorption. Both cases yield very similar final configurations, as listed in Table I, with a total energy difference of 0.02 eV. Because the optimized OPE thiolate is not precisely a bridge or a hollow site but roughly can be considered a near hollow site, we hereafter name it as a nontop adsorption site. Figure 3(b) shows the optimized OPE molecule on a nontop site of the Au(111) surface. The Au atoms right under the molecule are lifted up upon adsorption and others are rearranged so that the (111) plane is reconstructed. The equilibrium bond distances and bond angles are listed in Table I. The S atom equally binds with two nearest Au atoms at distances of 2.43 Å, much shorter than the S–Au distance in the top site adsorption. Moreover, unlike the top site OPE that stays perpendicular to the Au(111) surface, the lower part of hollow site adsorbed OPE tilts ~45° with respect to the Au surface, while the top part tilts ~15° less to the surface; hence the molecule appears to be bended near the gold surface. The adsorption geometry of thiolate bonded OPE thiols[46,47] or alkane[48,49] on the Au surface has been intensively studied, but there are still open questions[50] such as tilt angle, specific adsorption geometry, and especially the mobility of Au atoms under OPE adsorption. The tilt angle may depend on the side group and density of the molecules; it is now generally agreeable that different Au–S–C angles can be found in organic thiol adsorption. We think that the bending of OPE molecule is due to an insufficient vacuumed space, which yields a gradually reduced tilt angle above the lowest C atom that connects to S. This kind of bending may also be seen at low density SAM samples, where OPE intermolecular distances are ~10 Å.

B. Electronic properties

We then analyze the electronic properties of the OPE-Au(111) systems. Figure 4 shows the total density of states (DOS) of isolated OPE thiol, top site, and nontop site adsorbed OPEs to the Au(111) surface. Comparing the OPE thiol with OPE thiolate and Au systems, it can be found that the presence or increase of electron density of states around the Fermi level is due to the Au 5*d* and 6*s* contributions. The

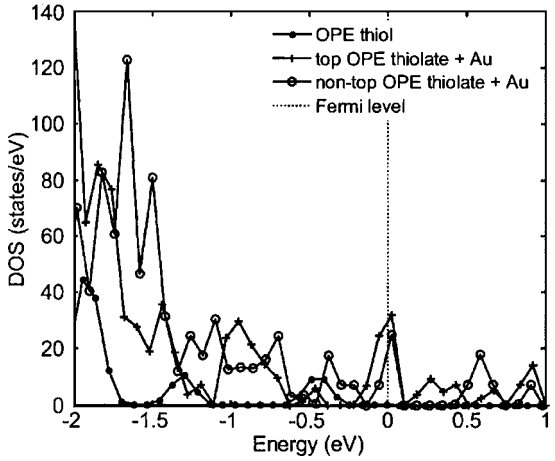

FIG. 4. Total DOS of isolated OPE thiol and OPE thiolate-Au(111) with top and nontop adsorption sites.

OPE–Au(111) systems are metallic, as indicated by the finite density of states at the Fermi level. DOS of Au in the nontop site adsorption is overall more hybridized due to the irregular surface reconstruction. It is also shown that the top site adsorbed system has a higher DOS at the Fermi level, indicating a better conductivity of the system along the Au surface, where a regular (111) surface structure is maintained.

Figure 5 depicts the projected DOS (PDOS) of the S atom contribution to the total DOS shown in Fig. 4 in order to investigate the S binding in different adsorption sites. The PDOS allows a description of the distribution of the electronic states in energy in terms of their original atomic character. It is shown in Fig. 5 that S in thiol has a well-localized electron density of states. Its highest DOS peak induced by *p* orbital appears at 0.7 eV below Fermi energy. This peak shifts to the Fermi level when S is placed on the top of the Au atom due to the electron density rearrangements with Au. This can be observed from the increased density at lower energies where the two small blue peaks are located. An almost continuously distributed DOS is observed in the case of the nontop binding site, resulting from the interactions between S and Au. This, on the other hand, implies a better conduction of the metal-molecule junction.

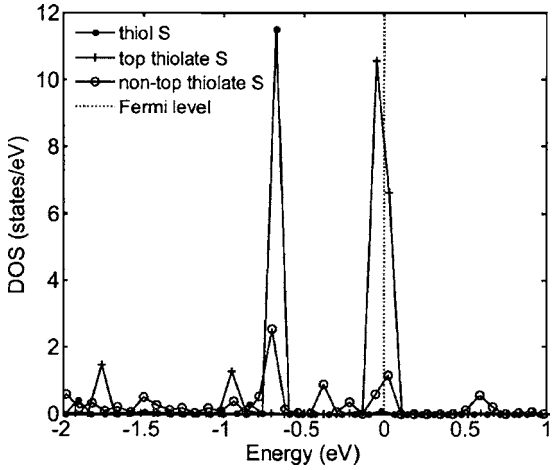

FIG. 5. Projected DOS of S atom in OPE thiol and top and nontop site adsorbed OPE thiolate.

Downloaded 25 Sep 2007 to 165.91.226.76. Redistribution subject to AIP license or copyright, see http://jcp.aip.org/jcp/copyright.jsp

TABLE II. Vibrational frequencies (cm^{-1}) of small molecules calculated with GGA-PW91 PAW potentials and comparison with other calculation and experiment.

Molecule		Expt.[a]	GGA-PW91[a]	GGA-PW91-PAW
CO		2170	2135	2141
CO_2		2349	2348	2391
		1388	1323	1333
		667	639	625
H_2O	B_2	3943	3528	3849
	$^2A_1$	3832	3721	3741
	A_1	1648	1590	1591
CH_4	$^2T_2$	3158	3086	3097
	A_1	3037	2973	2981
	E	1567	1515	1521
	T_2	1357	1292	1293

[a]Reference 57.

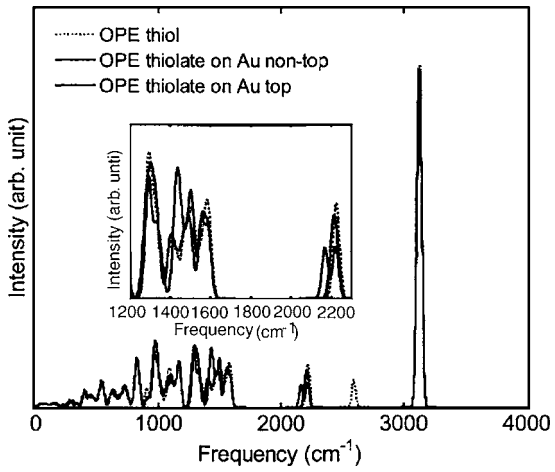

FIG. 6. Vibrational spectra comparison of isolated OPE thiol and OPE thiolate on top and nontop sites of the Au(111) surface. The insert zooms in the frequency between 1200 and 2300 cm^{-1}.

C. Vibrational frequency

Vibrational frequencies are determined from the Hessian matrix or force constant tensor (see, for instance, Ref. 51 for an explicit definition) constructed from the second derivative of the energy with respect to all pairs of Cartesian coordinates. In the VASP program, the calculations of the second derivatives are done numerically, using the forces obtained due to the small displacement of the nuclei along the x, y, and z directions. The Hessian matrix is a $3N \times 3N$ matrix, where N is the number of atoms. This matrix is then diagonalized, leading to a set of eigenvalues and eigenvectors. The vibrational frequencies are, apart from a constant factor, the square roots of $3N-6$ ($3N-5$ for linear system) highest eigenvalues of the Hessian matrix. In this work, a displacement of 0.02 Å is used, and only the high symmetry Γ point frequencies are considered.

Vibrational frequencies are calculated for the stretching mode of critical atoms in the OPE molecule, such as the triple bonded C atoms and atoms close to the Au surface, because they directly determine the morphology of the OPE on the Au surface,[33] and hence facilitate the calculation of various structural and electronic properties.

We first test the frequency calculations by comparing the results of small molecules with experimental and theoretical data calculated using the GGA-PW91. The results are listed in Table II. It is shown that the average deviations of GGAs from the experimental frequencies are about 4%. Results from the PAW potential show an overall improvement with respect to the ultrasoft pseudopotential calculations.

The same technique is used in the frequency calculations of OPE systems. Gold atoms are kept frozen at their equilibrium geometries for a better comparison of the frequency changes of the molecule on different adsorption sites. The 36 atoms in the asymmetric OPE thiolate yield 102 vibrational modes and 6 rotational and translational modes. Figure 6 shows the vibrational frequencies of isolated OPE thiol and OPE thiolate on two adsorption sites. The spectrum is convoluted with a Gaussian distribution. The intense peaks observed at 2599 and 3120 cm^{-1} are due to the S–H single bond and to the 13 C–H bonds in the OPE. The absence of peaks at ~2600 cm^{-1} in the OPE-Au systems is due to the thiolate formation. The two C–C triple bonds between the two phenyl rings resonate at 2225 cm^{-1} and the conjugated double bond stretching has a frequency around 1500 cm^{-1}. The lower frequencies below 1400 cm^{-1} correspond to angle bending, dihedral bending, and ring modes among others. For example, the C–H bending mode and the ring modes have been reported to be centered at 812 and 1089 cm^{-1}, respectively, using inelastic electron tunneling microscopy and other vibrational spectroscopies.[6,19] The same techniques also show that peaks between 400 and 600 cm^{-1} are associated with C–C–C in-plane bending. The lowest frequency part of the spectra tends to be very noisy due to phenyl twisting, molecular stretching in plane or out of plane of phenyl rings, and other vibration modes.[52]

The major difference between the top and nontop frequencies appears in the ~1500 and ~2200 cm^{-1}, dominated by the C–C double and triple bond stretching. The top site C–C triple bond frequency peak splits into two with equal intensity, indicating that the two C–C triple bonds have different stretching frequencies. This is suggested by the different bond lengths of C–C triple bonds in the top site adsorption, as reported in Table III. Table III lists vibrational

TABLE III. Vibartional frequencies (cm^{-1}) before and after adsorption on the Au surface.

	ω_{12}	ω_{23}	ω_{45}	ω_{67}	ω_{89}	ω_{1011}	ω_{SC}	ω_{SH}/ω_{SAu}
OPE thiol	1484	1419	2206	1501	2204	1483	1144	2599
OPE-Au top	1337	1525	2149	1501	2198	1482	1070	478
OPE-Au nontop	1401	1487	2190	1501	2199	1481	1146	417

Downloaded 25 Sep 2007 to 165.91.226.76. Redistribution subject to AIP license or copyright, see http://jcp.aip.org/jcp/copyright.jsp

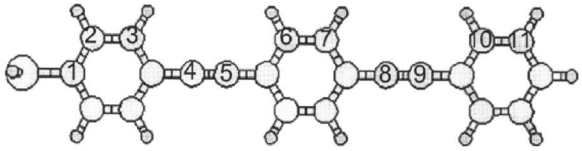

FIG. 7. Optimized OPE thiol molecule; the atom labels are used to report frequencies.

frequencies of some bonds along the molecule, as labeled in Fig. 7. Bonds that are far from Au surface (C6–C7, C8–C9, and C10–C11) have almost the same frequencies regardless of the adsorption site. However, frequencies of those near to the Au surface are much more affected. This is not only observed from the bond length difference, as listed in Table IV, but also from the different OPE adsorption geometries; bond angle and dihedral angle changes affect the frequency of the bond stretching as well. In general, the modes that affect most strongly the electrical properties (DOS) are characterized by the stretching motion of the C–C triple bonds, C–S bond, and S–Au bond. Depending on the number of bonded Au atoms and the S–Au distance, the S–Au stretching appears at a range from 416 to 477 cm^{-1}.

Figure 8 presents the spectra of two types of Au(111) surfaces, one adsorbed by OPE thiolate on the top site and the other on the nontop site. It is obvious that a nontop site adsorption induces a shift of two main vibrational modes of Au toward a lower frequency level. This is because of the significant surface reconstruction upon OPE binding, where a couple of Au atoms move out of the Au surface plane, and the Au–Au bond length increases. These changes soften the atomic force constant and strongly affect the local density of the surface atoms with lower frequencies. We suggest that the observed Au frequency shift can be used for the identification of adsorption site of the molecules.

D. Spin polarization

The magnetic properties of these systems have also been studied using spin polarized calculations. Recently, magnetic directed assembly has attracted interest for bringing many desirable properties to device fabrication, such as low damage, accurate replacement, and predictable orientation.[53–56] Actually, Naaman and co-workers[53,56] found experimentally that a unique occurrence of magnetism is shown when monolayers of organic molecule are self-assembled on Au substrates. Our calculations of the OPE-Au systems show that a net magnetic moment appears on either the molecule or Au surface, depending on the molecular adsorption site. As shown by magnetization density in Fig. 9, when adsorbed on the top site [Figs. 9(a) and 9(b)], the magnetic moment is concentrated on S and lower part of the molecule, particularly on the triple CC bonds. The net magnetic moment is $1.0\mu_B$, and very few spin density is observed on Au. This is simply because at a larger S–Au distance, S behaves as a radical and carries unpaired electron. As a matter of fact, this magnetic moment gradually decreases as we move the OPE thiolate closer to Au, as shown in Fig. 10. This can also be reflected from the nontop site adsorption case, where Au atoms instead of the OPE molecule carry most spin density and a relatively larger density is seen on S bonded Au atoms [Figs. 9(c) and 9(d)]. This is the result of the intensive electron interactions between S and Au, which at a great extent pairs the electrons in S radical. The total magnetic moment, in this case, is only $0.1\mu_B$, much smaller than that induced in the top adsorption site. Ideally, by applying an external magnetic field the adsorption site of OPE thiolate on Au surface could be manipulated when two or more species are used in the SAM.

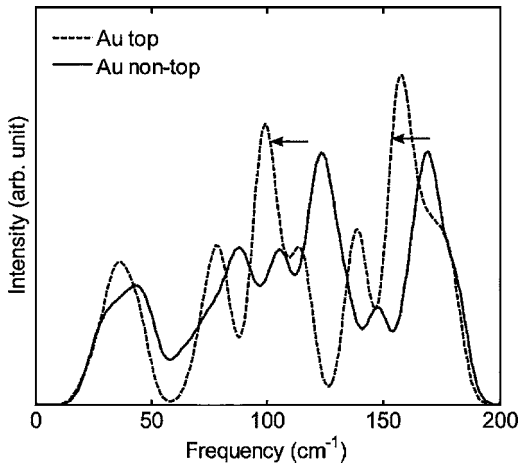

FIG. 8. Vibrational spectra of the Au surface with OPE thiolate on top and nontop sites.

IV. CONCLUSIONS

We have computed the morphology of single OPE molecule on different adsorption sites of Au(111) surface. The calculated systems are fully optimized with all the Au atoms unfixed. Using a plane-wave method, we have shown that a near-hollow site adsorption with two Au bindings (nontop site) is the most energetically favorable adsorption site. Unlike the top site adsorption, the nontop site adsorbed OPE thiolate forms a tilt angle of ~30° with respect to the surface. It also results in a severe surface reconstruction of Au, where two S bonded Au atoms are pulled out of the surface plane by the molecules. Vibrational spectra and critical bond frequency calculations indicate that Au supported OPE thiolates have different spectra, especially at C–C triple bond

TABLE IV. Lengths (Å) of bonds defined in Table I.

	d_{C12}	d_{C23}	d_{C45}	d_{C67}	d_{C89}	d_{C1011}	d_{SC}	d_{SH}/d_{SAu}
OPE thiol	1.402	1.390	1.221	1.385	1.221	1.391	1.790	1.352
OPE-Au top	1.432	1.376	1.228	1.381	1.222	1.392	1.695	3.89
OPE-Au nontop	1.406	1.388	1.222	1.385	1.221	1.392	1.768	2.44

Downloaded 25 Sep 2007 to 165.91.226.76. Redistribution subject to AIP license or copyright, see http://jcp.aip.org/jcp/copyright.jsp

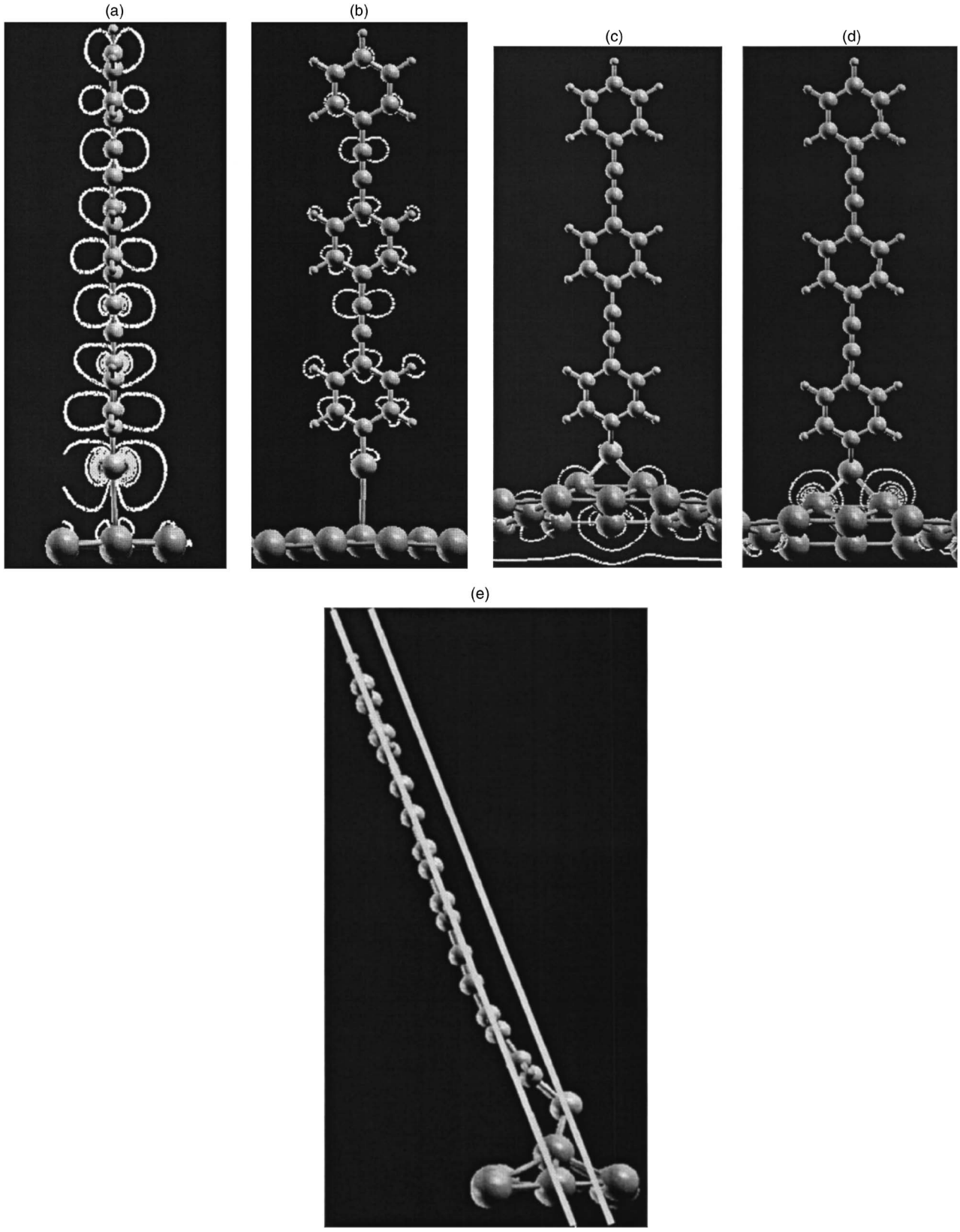

FIG. 9. (a) Magnetization density contour plot of top site adsorbed OPE thiolate on Au surface along the (001) direction. (b) Same plot as (a), but along the (010) direction. [(c) and (d)] Magnetization density contour plot for the nontop site adsorption along two planes shown in (e).

and C–C double bond stretching modes. Bonds near the surface are more affected by the adsorption locations than bonds far from the surface. Our calculations also show that nontop OPE thiolate adsorption lowers Au surface vibrational frequencies compared to the top site adsorption. In the end, we suggest that the shift of the frequency peaks may be used to identify the adsorption sites of the molecule on the Au surface. Also the on top configuration shows a strong spin im-

Downloaded 25 Sep 2007 to 165.91.226.76. Redistribution subject to AIP license or copyright, see http://jcp.aip.org/jcp/copyright.jsp

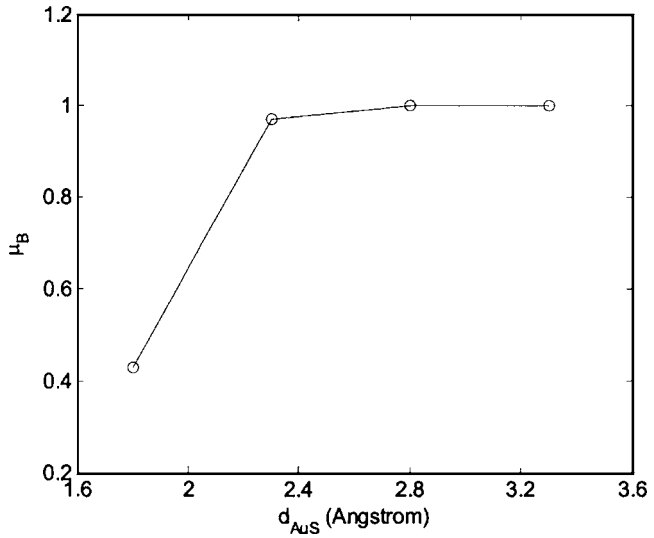

FIG. 10. Magnetic moment vs S–Au length varied in steps of 0.5 Å.

balance along the molecule and the nontop shows a small spin imbalance on the surface. This feature is of interest for the development of resonators for the detection of chemical and biological agents.

[1] J. Chen, M. A. Reed, A. M. Rawlett, and J. M. Tour, Science **286**, 1550 (1999).
[2] M. A. Reed, J. Chen, A. M. Rawlett, D. W. Price, and J. M. Tour, Appl. Phys. Lett. **78**, 3735 (2001).
[3] N. Gergel-Hackett, N. Majumdar, Z. Martin *et al.*, J. Vac. Sci. Technol. A **24**, 1243 (2006).
[4] J. M. Tour, Acc. Chem. Res. **33**, 791 (2000).
[5] A. Dhirani, P. H. Lin, P. GuyotSionnest, R. W. Zehner, and L. R. Sita, J. Chem. Phys. **106**, 5249 (1997).
[6] J. G. Kushmerick, J. Lazorcik, C. H. Patterson, R. Shashidhar, D. S. Seferos, and G. C. Bazan, Nano Lett. **4**, 639 (2004).
[7] Y. Selzer, L. T. Cai, M. A. Cabassi, Y. X. Yao, J. M. Tour, T. S. Mayer, and D. L. Allara, Nano Lett. **5**, 61 (2005).
[8] J. He, H. Chen, A. K. Flatt, J. J. Stephenson, C. D. Doyle, and J. M. Tour, Chem. Mater. **17**, 4832 (2005).
[9] L. Cai, M. A. Cabassi, H. Yoon, O. M. Cabarcos, C. L. McGuiness, A. K. Flatt, D. L. Allara, J. M. Tour, and T. S. Mayer, Nano Lett. **5**, 2365 (2005).
[10] L. H. Yu, Z. K. Keane, J. Ciszek, L. Chen, M. P. Stewars, J. M. Tour, and D. Natelson, Phys. Rev. Lett. **93**, 266802 (2004).
[11] J. M. Tour, Abstr. Pap. - Am. Chem. Soc. **227**, U265 (2004).
[12] M. P. Stewart, F. Maya, D. V. Kosynkin, S. M. Dirk, J. J. Stapleton, C. L. McGuiness, D. L. Allara, and J. M. Tour, J. Am. Chem. Soc. **126**, 370 (2004).
[13] J. M. Seminario, Y. Ma, L. A. Agapito *et al.*, J. Nanosci. Nanotechnol. **4**, 907 (2004).
[14] D. P. Nackashi, N. H. Di Spigna, D. A. Winick, C. J. Amsinck, L. Cheng, J. M. Tour, and P. D. Franzon, Nanotechnology **3**, 45–48 (2004).
[15] J. D. Monnell, J. J. Stapleton, J. J. Jackiw, T. Dunbar, W. A. Reinerth, S. M. Dirk, J. M. Tour, D. L. Allara, and P. S. Weiss, J. Phys. Chem. B **108**, 9834 (2004).
[16] D. K. James and J. M. Tour, Chem. Mater. **16**, 4423 (2004).
[17] L. Cheng, M. P. Stewart, F. Maya *et al.*, *Foundations of Nanoscience, Self-Assembled Architectures and Devices* (Science Technica, Washington, DC, 2004), pp. 199–203.
[18] J. G. Kushmerick, D. B. Holt, J. C. Yang, J. Naciri, M. H. Moore, and R. Shashidhar, Phys. Rev. Lett. **89**, 086802 (2002).
[19] D. P. Long, J. L. Lazorcik, B. A. Mantooth, M. H. Moore, M. A. Ratner, A. Troisi, Y. Yao, J. W. Ciszek, J. M. Tour, and R. Shashidhar, Nat. Mater. **5**, 901 (2006).
[20] A. Troisi and M. A. Ratner, Nano Lett. **6**, 1784 (2006).
[21] R. A. Hann, D. Bloor, and Royal Society of Chemistry (Great Britain) (Applied Solid State Chemistry Group), *Organic Materials for Nonlinear Optics* (Royal Society of Chemistry, Oxford, England, 1991), Vol. II.
[22] P. Wautelet, M. Moroni, L. Oswald, J. LeMoigne, A. Pham, J. Y. Bigot, and S. Luzzati, Macromolecules **29**, 446 (1996).
[23] Y. M. Zhao, Y. Shirai, A. D. Slepkov, L. Cheng, L. B. Alemany, T. Sasaki, F. A. Hegmann, and J. M. Tour, Chem.-Eur. J. **11**, 3643 (2005).
[24] M. Levitus, K. Schmieder, H. Ricks, K. D. Shimizu, U. H. F. Bunz, and M. A. Garcia-Garibay, J. Am. Chem. Soc. **123**, 4259 (2001).
[25] B. Tian, G. Zerbi, and K. Mullen, J. Chem. Phys. **95**, 3198 (1991).
[26] Y. G. Zhi, S. W. Lai, Q. K. W. Chan, Y. C. Law, G. S. M. Tong, and C. M. Che, Eur. J. Org. Chem. **2006**, 3125 (2006).
[27] A. V. Walker, T. B. Tighe, J. Stapleton, B. C. Haynie, S. Upilli, D. L. Allara, and N. Winograd, Appl. Phys. Lett. **84**, 4008 (2004).
[28] A. S. Blum, J. C. Yang, R. Shashidhar, and B. Ratna, Appl. Phys. Lett. **82**, 3322 (2003).
[29] M. P. Samanta, W. Tian, S. Datta, J. I. Henderson, and C. P. Kubiak, Phys. Rev. B **53**, R7626 (1996).
[30] J. M. Seminario, A. G. Zacarias, and J. M. Tour, J. Am. Chem. Soc. **122**, 3015 (2000).
[31] J. M. Seminario, A. G. Zacarias, and J. M. Tour, J. Am. Chem. Soc. **120**, 3970 (1998).
[32] J. M. Seminario and P. A. Derosa, J. Am. Chem. Soc. **123**, 12418 (2001).
[33] X. Yin, H. M. Liu, and J. W. Zhao, J. Chem. Phys. **125**, 094711 (2006).
[34] J. Taylor, M. Brandbyge, and K. Stokbro, Phys. Rev. B **68**, 115406 (2003).
[35] J. M. Seminario, A. G. Zacarias, and P. A. Derosa, J. Chem. Phys. **116**, 1671 (2002).
[36] G. Kresse and J. Hafner, Phys. Rev. B **47**, 558 (1993).
[37] G. Kresse and J. Hafner, Phys. Rev. B **49**, 14251 (1994).
[38] G. Kresse and J. Furthmuller, Comput. Mater. Sci. **6**, 15 (1996).
[39] G. Kresse and J. Furthmuller, Phys. Rev. B **54**, 11169 (1996).
[40] J. P. Perdew and Y. Wang, Phys. Rev. B **46**, 12947 (1992).
[41] P. E. Blochl, Phys. Rev. B **50**, 17953 (1994).
[42] G. Kresse and D. Joubert, Phys. Rev. B **59**, 1758 (1999).
[43] H. J. Monkhorst and J. D. Pack, Phys. Rev. B **13**, 5188 (1976).
[44] F. Schreiber, J. Phys.: Condens. Matter **16**, R881 (2004).
[45] B. J. Schwartz, Annu. Rev. Phys. Chem. **54**, 141 (2003).
[46] W. S. V. Kwan, L. Atanasoska, and L. L. Miller, Langmuir **7**, 1419 (1991).
[47] Z. Zhang, T. L. Beck, J. T. Young, and F. J. Boerio, Langmuir **12**, 1227 (1996).
[48] H. Sellers, A. Ulman, Y. Shnidman, and J. E. Eilers, J. Am. Chem. Soc. **115**, 9389 (1993).
[49] F. Schreiber, Prog. Surf. Sci. **65**, 151 (2000).
[50] K. Walzer, E. Marx, N. C. Greenham, R. J. Less, P. R. Raithby, and K. Stokbro, J. Am. Chem. Soc. **126**, 1229 (2004).
[51] J. M. Seminario, Int. J. Quantum Chem. **60**, 59 (1996).
[52] A. Pecchia, M. Gheorghe, A. Di Carlo, P. Lugli, T. A. Niehaus, T. Frauenheim, and R. Scholz, Phys. Rev. B **68**, 235321 (2003).
[53] I. Carmeli, G. Leitus, R. Naaman, S. Reich, and Z. Vager, J. Chem. Phys. **118**, 10372 (2003).
[54] Z. Vager, I. Carmeli, G. Leitus, S. Reich, and R. Naaman, J. Phys. Chem. Solids **65**, 713 (2004).
[55] D. P. Long, C. H. Patterson, M. H. Moore, D. S. Seferos, G. C. Bazan, and J. G. Kushmerick, Appl. Phys. Lett. **86**, 153105 (2005).
[56] R. Naaman and Z. Vager, Phys. Chem. Chem. Phys. **8**, 2217 (2006).
[57] D. C. Patton, D. V. Porezag, and M. R. Pederson, Phys. Rev. B **55**, 7454 (1997).

Downloaded 25 Sep 2007 to 165.91.226.76. Redistribution subject to AIP license or copyright, see http://jcp.aip.org/jcp/copyright.jsp